J. Appl. Comput. Mech., 6(1) (2020) 145-159
DOI: 10.22055/JACM.2019.28771.1511

ISSN: 2383-4536
jacm.scu.ac.ir

M&MoCS

Shahid Chamran University of Ahvaz

Journal of Applied and Computational Mechanics

Research Paper

Analysis of High-order Approximations by Spectral Interpolation Applied to One- and Two-dimensional Finite Element Method

Luís Philipe Ribeiro Almeida[1], Hilton Marques Souza Santana[2], Fabio Carlos da Rocha[3]

[1] *Federal University of Alagoas, Laboratory of Scientific Computing and Visualization Technology Center*
Campus A.C. Simões, Maceió-AL, 57092-970, Brazil, Email: luis.almeida@ctec.ufal.br
[2] *Federal University of Sergipe, Department of Civil Engineering*
Campus São Cristovão, Aracaju-SE, 49100-000, Brazil, Email: hiltonmarquess@gmail.com
[3] *Federal University of Sergipe, Department of Civil Engineering*
Campus São Cristovão, Aracaju-SE, 49100-000, Brazil, Email: fcrocha@ufs.br

Received March 09 2019; Revised May 07 2019; Accepted for publication May 20 2019.
Corresponding author: Fabio Carlos da Rocha (fcrocha@ufs.br)
© 2020 Published by Shahid Chamran University of Ahvaz
& International Research Center for Mathematics & Mechanics of Complex Systems (M&MoCS)

Abstract. The implementation of high-order (spectral) approximations associated with FEM is an approach to overcome the difficulties encountered in the numerical analysis of complex problems. This paper proposes the use of the spectral finite element method, originally developed for computational fluid dynamics problems, to achieve improved solutions for these types of problems. Here, the interpolation nodes are positioned in the zeros of orthogonal polynomials (Legendre, Lobatto, or Chebychev) or equally spaced nodal bases. A comparative study between the bases in the recovery of solutions to 1D and 2D elastostatic problems are performed. Examples are evaluated, and a significant improvement is observed when the SFEM, particularly the Lobatto approach, is used in comparison to the equidistant base interpolation.

Keywords: Spectral finite element method; Elastostatic problem; Orthogonal basis.

1. Introduction

The finite element method (FEM) is among the most commonly used numerical methods for solving differential equations. In this method, most of the functions used are low-order polynomial approximation functions [1]. However, significant errors can appear when complex geometries or loadings with rapidly varying intensity need to be reproduced depending on the polynomial order and the nodal base employed [2, 3, 4]. The high-order FEM is a method to overcome difficulties in the modeling of complex problems, be it geometric or of boundary condition, where obtaining the numerical solution is difficult due to its computational or theoretical characteristics [5]. From the computational perspective, the choice of bases influences the stability and accuracy of the procedures used to determine the numerical solution [6]. In general, one of the main issues when applying high-order polynomial functions to interpolate (or to construct numerical solutions of partial differential equations), is the appropriate selection of values for the nodal distribution points to overcome the effects of Runge phenomenon [7]. The Runge phenomenon can appear in high-order polynomial interpolation with equally nodal bases, and is characterized by large oscillations at the ends of the interpolation interval [8]. To overcome this effect, several studies have shown that the choice of nodal points constructed from the zeros of orthogonal polynomials are optimal (or near-optimal) bases that decreases or eliminates these oscillations (Runge effect) in the interpolation process [9].

Published online: July 15 2019

The development of FEM elements from high-order polynomial interpolation with the nodal points formed from the zeros of the orthogonal polynomials constitute the spectral finite element method (SFEM) [3]. This method combines the classical approach of FEM with high-order spectral elements exhibiting exponential convergence characteristics. Several previous studies have used spectral expansions, mainly in fluid dynamics [10,11,12] and wave propagation problems [3, 4, 7], where the geometric flexibility of the finite element type "h" is combined with the resolution properties of the spectral methods. The influence of node distribution (Lobatto, Chebyshev, and equidistant) and the order of the approximation polynomial (Lagrange) when applied to 1D numerical problems related to the propagation of waves in bars was analyzed by Zak and Krawczuk [3]. The application of SFEM in structural integrity monitoring through ultrasonic guided waves was studied by Willberg et al. [7]. The efficiency and precision of spectral elements based on Legendre's and Lagrange's polynomial approximations (p-FEM) and isogeometric elements based on rational non-uniform B-splines (NURBS, N-FEM) were analyzed.

In the field of solids mechanics analysis, SFEM is seen as one of the main approaches to modeling of wave propagation problems. The applicability of this spectral approach to solving static problems however, remains less explored, due to its increased mathematical complexity and computational cost. Several studies, such as the work done by Tai and Chan [13], have explored the use of Legendre spectral approach in modeling Timoshenko beam elements in static and dynamics analysis. Dauksher and Emery [14] used Chebyshev spectral functions in the analysis of static and dynamics problems in two dimensions, and more recently, Khaji and Zakian [15] proposed the SFEM as a new tool in the quantification of uncertainties.

Man et al. [16] used the spectral elements in the analysis of bending in plates. Man et al. [17] employed the high-order spectral elements in the study of piezoelectric plates, producing satisfactory results with minimal high-order elements, and more recently, Lin et al. [18] showed the applicability of the method in the analysis of composite laminates and sandwich plates.

Nogueira et al. [6] applied SFEM to static problems related to structural mechanics in linear and nonlinear elastic regimes and compared some hierarchical bases in the literature. As a comparison, the condition number resulting from the solution to the Poisson problem with homogeneous Dirichlet conditions was considered. In implementing SFEM, the Lagrange polynomials interpolated at Gauss–Jacobi quadrature points were used and the resulting analysis were very promising for solving linear and nonlinear elasticity problems.

Zak and Krawczuk [19] studied some static and modal problems of isotropic shell structures such as transverse deformation using SFEM. In the development of SFEM, the orthogonal polynomials of Lobatto and the quadrature of Gauss-Lobatto-Legendre were used. The static and/or modal responses were compared with the analytical solutions present in the literature. Consequently, the application of SFEM to the shell problem provided a significant reduction in the numerical errors; hence, improved accuracy was achieved compared to conventional FEM. Wang and Sprague [20] used the Legendre spectral finite elements for analyzing geometric linear and nonlinear elastic deformations of composite beams. In that study, nodal points located in the Gauss-Lobatto-Legendre quadrature positions were used and interpolated through Lagrange polynomials.

Unlike previous studies on the behavior of static structures using SFEM, the present work focuses on a comparative study, in both accuracy and computational cost, between the orthogonal bases (Lobatto, Chebyshev and Legendre), the equidistant base and the standard FEM (equidistant base with a low degree) in recovering the solution to 1D and 2D static problems using SFEM. Specifically, our 1D analysis uses Lagrangian interpolation at equally spaced points within the validity range as well as in the zeros of the Lobatto, Legendre, and Chebyshev polynomials. For the 2D analysis, triangular spectral elements constructed from Proriol polynomials [21] are used in two variables which are interpolated at equally spaced points and in the zeros of the symmetrized Lobatto polynomial in the triangular domain of reference. Subsequently, the spectral approximations are used in conjunction with the FEM to analyze a beam problem subjected to rapid spatial variation loading and another 2D problem with complex geometry and rapid spatial variation loading.

2. High-order Approximation in One Dimension

To improve the automation of the numerical calculation regardless of the size and degree of distortion of each element, the dimensionless space $[-1,1]$ is adopted for isoparametric mapping of coordinates and in the generation of the interpolation functions used in SFEM.

2.1. Generalized Vandermond matrix

Let the set of points, which depend on the polynomial order, be generated from the base of the dimensionless space. The general term of the interpolator polynomial in imposing the cardinality's propriety is written as [2]

$$\Psi_i(\xi) = \sum_{j=0}^{m} a_{ij}\xi^j = a_{i0} + a_{i1}\xi + \ldots + a_{im}\xi^m = \delta_m^i \tag{1}$$

or

$$\underbrace{\begin{bmatrix} a_{10} & \cdots & a_{1m} \\ \vdots & \ddots & \vdots \\ a_{k0} & \cdots & a_{km} \end{bmatrix}}_{M} \underbrace{\begin{bmatrix} 1 & \cdots & 1 \\ \vdots & \ddots & \vdots \\ \xi_1^m & \cdots & \xi_k^m \end{bmatrix}}_{V} = \underbrace{\begin{bmatrix} 1 & \cdots & 0 \\ \vdots & \ddots & \vdots \\ 0 & \cdots & 1 \end{bmatrix}}_{I} \tag{2}$$

where, Ψ_i is the shape function evaluated at $i=1,\ldots,(m+1)$, δ_m^i is the Kronecker delta and a_{ij} are the polynomial coefficients of the. The matrix V is called the matrix of Vandermonde.

$$MV = I \tag{3}$$

2.2. Nodal bases

The choice of interpolating base has great importance when one needs to obtain the approximation function to resolve a physical problem. This is because of the direct interference of the numerical procedure accuracy, either through errors in the geometric representation or those obtained in the mechanical response of the problem.

2.2.1. Equidistant nodal bases

In order to construct a set of uniform points, the range of points as $\{\xi_k \epsilon\ \mathbb{R}; -1 \le \xi_k \le +1\}$ is used for the mapping the bases of the dimensionless space. The set is obtained through [23]:

$$\xi_k = \xi_1 + r(k-1) \tag{4}$$

where $k=1,\ldots,(m+1)$ is the partition of the interval, $\xi_1 = -1$ (the starting point), $r = 2/m$ is the ratio of arithmetic progression, and m is the order of interpolation.

2.3. Spectral bases

The spectral method is centered on the appropriate selection of base functions, which will lead to a solution with high convergence rate of a polynomial [14]. The combination of this approach with the discretization of the FEM, allows for a stable solution with high precision which removes limitations on the geometry's domain with a significant decrease in the required mesh [15]. The choice of the orthogonal polynomials, as the function bases proved to be effective when the polynomials of Chebyshev [14], Lobatto [15, 19] and Legendre [13, 20], were chosen for static analysis with FEM.

Spectral expansions are used to ensure convergence in the numerical analysis of engineering problems thanks to the high degree (m) of approximation. Unlike other approximations, the spectral approach tries to guarantee the decrease of numerical error with a faster rate than any $1/m$ power [23].

In the spectral interpolation approach, the interior nodes are positioned at the zeros of the orthogonal polynomials. The dimensionless space of the set points are determined in the range of $[-1,1]$, having $\xi_1 = -1$ and $\xi_{m+1} = 1$ as extreme nodes, moreover, the m-zeros of polynomials as internal nodes.

The followings are the families of orthogonal polynomials, as well as the recurrence formulas used in this study.

2.3.1. Lobatto's spectral base

The corresponding distribution of the zeros of Lobatto polynomials is optimal for 1D interpolation, considering that one node is placed at the right-end and another at the left-end [22]. The recurrence function of Lobatto's polynomials is presented in Eq. (5) [23].

$$Lo_{m+1}(\xi) = \frac{1}{2^{i+1}(i+1)!}\frac{d^{i+2}}{d\xi^{i+2}}(\xi^2-1)^{i+1} = \frac{i(2(i+1))!}{2^{i+1}(i+1)!}\xi^i \tag{5}$$

2.3.2. Legendre's spectral base

Legendre polynomials are also defined in the interval $[-1,1]$ as the Lobatto polynomials. The recurrence function of Legendre's spectra base is showed in Eq. (6) [13].

$$L_m(\xi) = \frac{1}{2^m(\mathrm{m})!}\frac{d^m}{d\xi^m}(\xi^2-1)^m = \frac{(2m)!}{2^m m!}\xi^m \tag{6}$$

2.3.3. Chebyshev's spectral base

One of the most effective in elastostatic problems [14] is the distribution based on the polynomials of Chebyshev, C_m. Like the other orthogonal polynomials presented here, the Chebyshev polynomial has the definition domain in $[-1,1]$ and the range of variation $|C_i(\xi)| \le 1$ with $-1 \le \xi \le 1$. The Chebyshev recursive relation is presented in Eq. (7) [24]:

$$C_{m+1}(\xi)=2\xi\ C_m(\xi)-\ C_{m-1}(\xi),\ \mathrm{m}\geq 1 \tag{7}$$

with $C_0(\xi)=1$ and $C_1(\xi)=\xi$.

3. High-order Approximation in Triangular Domain

Let us consider a polynomial interpolation for functions with two variables in the triangular domain contained in the physical space (plane xy). The triangle contained in the physical space is mapped to a standard right isosceles triangle contained in the parametric plane $\xi_1-\xi_2$, such that $0\leq\xi_1\leq 1$, $0\leq\xi_2\leq 1-\xi_1$, and an arbitrarily chosen vertex is mapped to the origin.

Throughout the interpolation process, Lagrange-like cardinal nodal interpolation functions are introduced, $\psi(\xi_1,\xi_2)$, for $i=1,2,\ldots,N$, with the following property:

$$\psi_i(\xi_1^j,\xi_2^j)=\delta_{ij} \tag{8}$$

where δ_{ij} is the Kronecker delta.

The interpolation of a function $f(\xi_1,\xi_2)$ is performed through a polynomial expansion with degrees of m over the area of the triangle contained in the dimensionless space, as follows:

$$f(\xi_1,\xi_2)=\sum_{j=1}^{N} f_i(\xi_1,\xi_2)\psi_i(\xi_1,\xi_2) \tag{9}$$

where $f_i(\xi_1,\xi_2)$ is the presumed-known function values at each of the $N=(m+1)(m+2)/2$ nodes, with m being the degree of approximation.

Next, to compute the functions of cardinal nodal interpolation, a set of N polynomial functions, $\phi_j(\xi_1,\xi_2)$, which forms a complete base for the polynomial space of order m, is introduced as follows:

$$\psi_i(\xi_1,\xi_2)=\sum_{j=1}^{N} c_j^i\phi_j(\xi_1,\xi_2) \tag{10}$$

where c_j^i indicates unknown coefficients. By substituting Eq. (8) into Eq. (10), we can determine the unknown coefficients, c_j^i, as follows:

$$\psi(\xi_1,\xi_2)=\phi(\xi_1,\xi_2).\left[V_\phi\right]^{-1} \tag{11}$$

where V_ϕ is Vandermonde's generalized matrix (Eq. (2)), with components $V_{\phi_i}=\phi_i(\xi_1^j,\xi_2^j)$.

3.1. Proriol's polynomial base

A standard triangle is mapped from the parametric $\xi_1-\xi_2$ plane to the standard square $-1\leq\xi_1^{'}\leq 1$, $-1\leq\xi_2^{'}\leq 1$ (Fig. 1), using the Duffy transformation:

$$\xi_1^{'}=\frac{2\xi_1}{1-\xi_2}-1,\xi_2^{'}=2\xi_2-1 \tag{12}$$

According to [23], a more desirable base is constituted using Proriol's polynomial, which is totally orthogonal over the triangular domain. Proriol's polynomial, PR_{kl}, involves monomials of the form $\xi_1^p\xi_2^{(j-p+q)}$ with the order of $k+q$ and with $p=1,2,\ldots,k$ and $q=1,2,\ldots,l$, such that

$$PR_{kl}=\left[\sum_{i=0}^{k}\binom{k}{i}\binom{k}{k-i}\left(\frac{\xi_1^{'}-1}{2}\right)^{k-i}\left(\frac{\xi_1^{'}+1}{2}\right)^{i}\left(\frac{1-\xi_2^{'}}{2}\right)^{k}\right].\left[\sum_{j=0}^{l}\binom{l+2k+1}{j}\binom{l}{l-j}\left(\frac{\xi_2^{'}-1}{2}\right)^{l-j}\left(\frac{\xi_2^{'}-1}{2}\right)^{j}\right] \tag{13}$$

3.2. Equally spaced nodal distribution

To obtain the degree interpolator polynomial m, the equally spaced distribution (Fig. 2) is given as [24]

$$\xi_1^i=v_i,\quad \xi_2^j=1-v_{m+2-j} \tag{14}$$

where $v_i=(i-1)/m$ indicates the dimensionless points for $i=1,2,\ldots,m+1$ and $j=1,\ldots,m=2-i$.

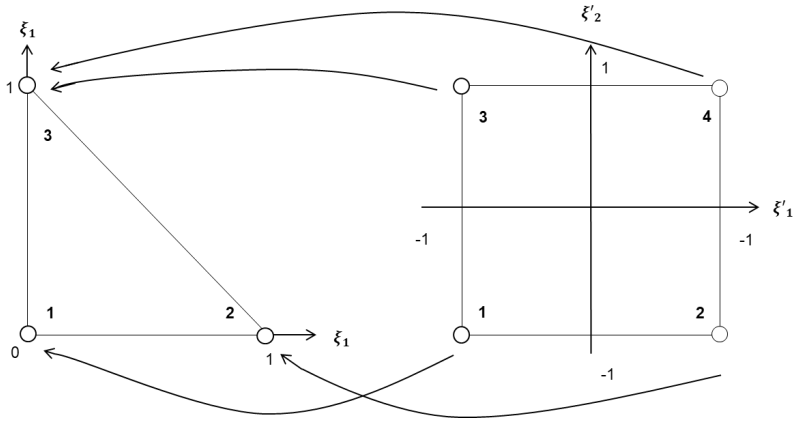

Fig. 1. Mapping from the square to the standard triangle using the Duffy transform

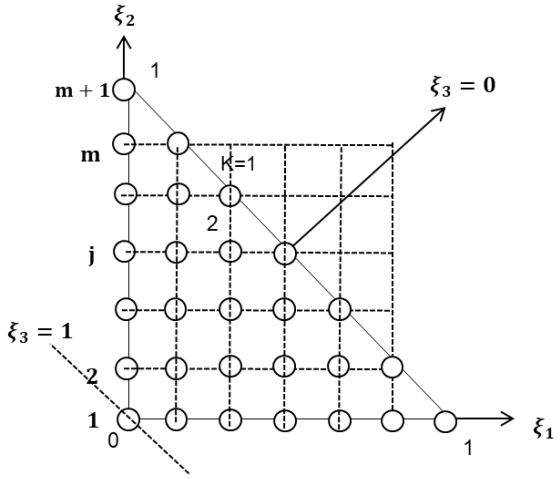

Fig. 2. Equally spaced distribution on the triangle

3.3. Symmetrized spectral nodal base

As proposed in ref. [23], in this study, the following triangular distribution of Lobatto endowed with three-fold rotational symmetry is used:

$$\xi_1^i = \frac{1}{3}\left(1+2v_i - v_j - v_k\right), \quad \xi_2^j = \frac{1}{3}\left(1+2v_j - v_i - v_k\right) \tag{15}$$

where $i = 1,\ldots,m+1$, $k = m+3-i-j$ and $j = 1,\ldots,m+2-i$, $v_1 = 0$, $\mathrm{v}_i = \left(1+t_{i-1}\right)/2$ and $\mathrm{v}_{m+1} = 1$ are non-dimensional points, where t_i for $i = 2,3,\ldots,m$ are the zeros of the orthogonal polynomials (Lobatto, Legendre, or Chebyshev) of degree $m-1$ distributed in the interval $[-1,1]$.

4. Lebesgue Constant and Condition Number

To begin with the study of the Lebesgue constant, it is necessary to define an error quantification, called the max norm. The max norm of a function $f(\mathrm{x})$, denoted by $\|f(x)\|$, is defined as the maximum absolute value $f(x)$ over an interpolation interval [2]. Defining the max norm in interpolation, it is possible to determine an optimal polynomial, $P_N^{oti}(x)$, which holds the minimum error for the max norm $\|e(x)\|$, called the minimax error and written as $p_N[f(x)]$. To calculate $\|e(x)\|$, consider a function $f(x)$, which is interpolated by $P_N(x)$. The difference between the exact function and the approximation is given as follows:

$$e(x) = P_N(x) - f(x) \tag{16}$$

For the calculation of the maximum norm $\|e(x)\|$, the set of all functions $f(x)$ with the unit max norm, $\|f(x)\| = 1$, is considered. The corresponding norm of the interpolation error is [2]

$$\begin{aligned}\|e(x)\| &= \|P_N(x) - f(x)\| = \|(P_N(x) - P_N^{oti}(x)) + (\mathrm{P}_N^{oti}(x) - f(x)\| \\ &\leq \|P_N(x) - P_N^{oti}(x)\| + \|P_N^{oti}(x) - f(x)\| = \|P_N(x) - P_N^{oti}(x)\| + p_N[f(x)]\end{aligned} \tag{17}$$

Then, the Lebesgue lemma is applied [5]. To emphasize that the polynomial $P_N(x)$ is an approximation of the function $f(x)$, the notation $P_N(x, f)$ is used, and the inequality is developed as follows:

$$\|P_N(x,f) - P_N^{oti}(x)\| = \|P_N(x,f) - \mathrm{P}_N(x, P_N^{oti})\| \leq \|P_N\| \|f(x) - P_N^{oti}(x)\| \tag{18}$$

where $\|P_N\| \equiv Max\left(\|P_m(f(x))\|\right)$ is calculated for all functions, $f(x)$. It is possible to rewrite Eq. (18) as

$$\|e(x)\| \leq (1 + \|P_N\|) p_N[f(x)] \tag{19}$$

Thus, the limit for norm $\|P_N\|$ is obtained [5]

$$\|P_N\| \equiv Max\left(\left|\sum_{i=1}^{N+1} f(x_i)\psi_i(x)\right|\right) \leq Max\left(\sum_{i=1}^{N+1} |f(x_i)||\psi_i(x)|\right) \leq Max(\Im_N(x)) \tag{20}$$

where $\Im_N$ is the Lebesgue function. The maximum value of the Lebesgue function is the Lebesgue constant [5]:

$$\Im_N(x) \equiv \sum_{i=1}^{N+1} |\psi_i(x)|, \Lambda_N \equiv Max(\Im_N(x)) \tag{21}$$

The combination of Eqs. (21) and (19) reveals that the interpolation convergence properties depend on the minimax error and the Lebesgue constant in the polynomial order.

A problem is said to be well-conditioned when large perturbations in the data cause small disturbances in the linear system solution. On the contrary, when small perturbations in the data cause significant disturbances in the results, it is said that this is a poorly conditioned problem. One way to quantify this feature is given by the condition number analysis. Thus, the lower the number of conditions, the better is the conditioning of the problem [25]. The condition number of a matrix A is defined as

$$cond(\mathrm{A}) = \|A\| \left\|A^{-1}\right\|, \|A\|_E = \sqrt{\sum_{i,j=1}^{m} \xi_{ij}^2} \tag{22}$$

where a_{ij} indicates the coefficients of matrix A.

To quantify the error associated with the use of high-order approximations, consider a function $f(x)$, which is interpolated by polynomial $P_m(x)$, of equal or lesser degree m, the relative error is given by

$$Error = \frac{|P_m(x) - f(x)|}{|P_m(x)|} \tag{23}$$

5. Formulation of 1D and 2D FEM

The FEM formulation is performed through the principle of virtual work (PVW) applied to both 1D and 2D problems, as [18]

$$\int_{V^{(e)}} \delta\varepsilon^T \boldsymbol{\sigma} dV = \oint \delta \mathbf{u}^T \mathbf{q} t dS + \sum_{i=1}^{r} \delta \mathbf{u}_i \mathbf{f}_i \tag{24}$$

The terms on the r.h.s. of Eq. (24) represent the virtual work of the surface tractions $\boldsymbol{q}$ and the external point load $\boldsymbol{f}_i$. The integral on the l.h.s. represents the work performed by stress $\boldsymbol{\sigma}$ over the virtual strain $\delta\boldsymbol{\varepsilon}$. The displacement fields are given by $\delta\boldsymbol{u}$ and $\delta\boldsymbol{u}_i$ for point displacements.

From the integral formulation, Eq. (24), the finite element discretization of any order is performed, which provides the system of equations:

$$[k]\{d\} = \{f\} \tag{25}$$

where $[k] = \sum_{e=1}^{N} [k^e]$ is the stiffness matrix of the system and $\{f\} = \sum_{e=1}^{N} \{f^e\}$ is the vector of global forces. According to beam theory the elementary stiffness matrix and the force vector are expressed as [26]

$$\left[K^e\right]=\int_{-1}^{1}(EI)^e\left[B^e\right]^T\left[B^e\right]J(\xi)d\xi\ ,\ \ \left\{f^e\right\}=\int_{-1}^{1}[\psi]^T\,q(x)J(\xi)d\xi \tag{26}$$

where $[\psi]$ is the shape function matrix of the beam element (1D), $\left[B^e\right]$ is the vector containing the second derivative of the shape functions, and $J(\xi)$ is the Jacobian function of the transformation. The shape functions of the beam element are obtained by Hermite interpolation at the nodal points in the zeros of orthogonal polynomials presented in sect. 2.3. For 2D problems, the elementary stiffness matrix and the force vector are expressed as [26]

$$\left[K^e\right]=\iint_T[B]^T[D][B]tJ(\xi_1,\xi_2)d\xi_1d\xi_2\ ,\ \ \left\{f^e\right\}=\oint_{l^{(e)}}[\psi]^T\{\mathbf{t}\}tJ(\xi)d\xi \tag{27}$$

where T is a dimensionless $\xi_1-\xi_2$ standard triangle and t is its thickness. For plane stress problems, t is the actual thickness of the solid. In plane strain situations, the analysis domain is a unit slice and t is equal to one. The $[B]$ term is

$$[B]=\begin{bmatrix}B_1 & B_2 & B_3 & \dots & B_N\end{bmatrix},\ B_i=\begin{bmatrix}\dfrac{\partial\psi_i}{\partial x} & 0\\ 0 & \dfrac{\partial\psi_i}{\partial y}\\ \dfrac{\partial\psi_i}{\partial y} & \dfrac{\partial\psi_i}{\partial x}\end{bmatrix} \tag{28}$$

and

$$[D]=\begin{bmatrix}d_{11} & d_{12} & 0\\ d_{21} & d_{22} & 0\\ 0 & 0 & d_{33}\end{bmatrix} \tag{29}$$

is the elastic material matrix (or constitutive matrix). For plane stress $d_{11}=d_{22}=E/(1-\nu^2)$, $d_{33}=E/[2(1+\nu)]=G$, $d_{12}=d_{21}=\nu d_{11}$, and for plane strain $d_{11}=d_{22}=E(1-\nu)/[(1+\nu)(1-2\nu)]$, $d_{12}=d_{21}=d_{11}\nu/(1-\nu)$, $d_{33}=E/[2(1+\nu)]=G$, where G and E are the transverse and longitudinal moduli of elasticity, respectively, and ν is the Poisson ratio. Thus, $[k]=\sum_{e=1}^{N}\left[k^e\right]$ is the stiffness matrix of the system and $\{f\}=\sum_{e=1}^{N}\left\{f^e\right\}$ is the vector of global forces, with $\left\{f^e\right\}=\oint_{l^{(e)}}[\psi]^T\{t\}tds$ being the equivalent nodal force vector originating from surface tractions.

6. Numerical Results

Numerical examples are presented to analyze the influence of the nodal bases (presented in the previous sections), considering the reproduction of geometries and representation of physical problems for 1D and 2D solids by FEM.

6.1. Mapping of 1D function with rapid increases

In order to illustrate the efficiency of spectral interpolation in recovering the geometries with complex characteristics, the following approximation of the analytical function is considered:

$$\mathrm{F}(x)=\frac{1}{1+25x^2} \tag{30}$$

Fig. 3 shows that the equally spaced base deteriorates more rapidly compared with the orthogonal bases as the polynomial order is increased. This poor performance is located in the regions near the ends of the interpolated element, and is explained through the Runge phenomenon. The quantification of the deterioration of the equidistant base can be seen in Fig. 4a, which plots the Lebesgue constant against the degree of the interpolator polynomial. Fig. 4b presents a treatment of the error by the Euclidean norm (condition number) of the Vandermonde matrix, showing an accentuated growth for the equally spaced nodal base when compared to the other bases. Table 1 quantitatively presents the values of the Lebesgue constant with an increase in the polynomial order. It is shown in Table 1 that the equidistant base presents unlimited values when compared to the orthogonal bases of Legendre, Chebyshev, and Lobatto, which guarantees better efficiency in the interpolation to orthogonal bases.

6.2. Mapping of the rapidly increasing function in triangular domain

To demonstrate the interpolation strategies presented for a triangular element, the interest function defined in Eq. (31) is mapped. This function has a validity domain over the equilateral triangle of unit sides and $(\hat{\xi}_1^c,\hat{\xi}_2^c)=(1/2,\sqrt{3}/6)$ is the

centroid of the triangle. The results obtained with the distribution at the orthogonal base nodes using the Proriol interpolator polynomial are compared with those of the equidistant distribution. Unsatisfactory performance is observed through Fig. 5 in case of a high polynomial order when using uniformly spaced points. In Fig. 5, it is observed that the equally spaced points do not guarantee convergence as the order of the approximation is increased, i.e., the order of approximation of 20 provided better results compared to that of 40. However, fine performance is observed when the bases formed by the families of the orthogonal polynomials are used.

$$\mathrm{F}(\hat{\xi}_1,\hat{\xi}_2)=\frac{1}{1+25(\hat{\xi}_1-\hat{\xi}_1^c)}\frac{1}{1+25(\hat{\xi}_2-\hat{\xi}_2^c)}. \tag{31}$$

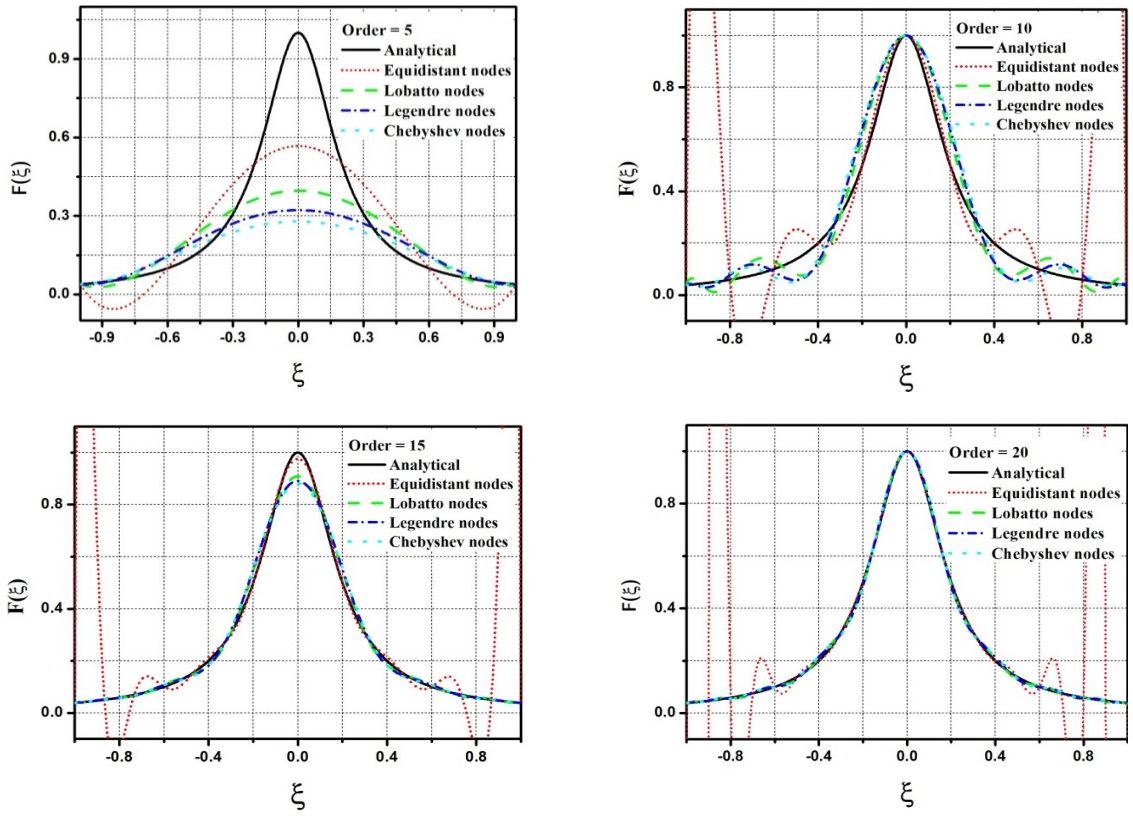

Fig. 3. Dependence of nodal base on the representation of functions with rapid increases.

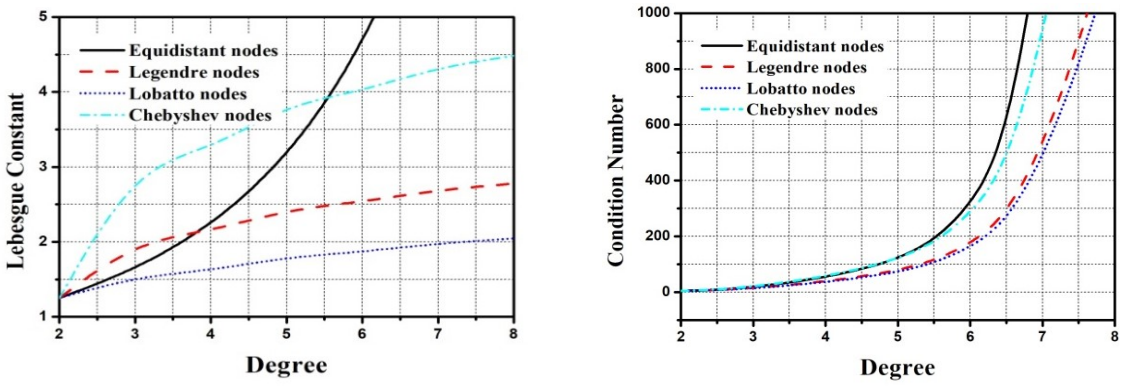

(a) (b)

Fig. 4. Lebesgue constant (a) condition number (b).

6.3. Applications

In this section, two problems are presented and three analyses are performed. The 1D and 2D analyses are performed for a simply supported beam and a one subjected to a loading with rapid increases. The third analysis is related to the 2D elastostatic problem of a mechanical gear subjected to a loading with rapid increases. In the 1D analysis of the simply supported beam, the modulus of elasticity (E), moment of inertia (I), and thickness are all unitary, with compatible units.

Other values of the mechanical constants are reported in the following examples. In all analyses, the spectral bases are used together with FEM. In order to evaluate the computational cost between nodal bases, the CPU time study was implemented in FORTRAN and all numerical analysis were done on a machine with Intel ® Core™ i7-6500U CPU, 2.5GHz with 4 cores and 4 logical Processors and 16 GB of RAM.

6.3.1. Discretization of the simply supported beam: a 1D approach

For the 1D approach, a simply supported beam (Fig. 6a) is subjected to a distributed load with intensity given by Eq. (30). In the numerical analysis, a single-beam finite element is used in the discretization of the problem and the polynomial order is increased for each previously presented nodal base. Fig. 6b shows a graph of the beam's maximum displacement error as the degree of approximation is increased. Fig. 6b also depicts the low performance of the equally spaced base when attempting to recover the analytical displacement field, although this one has a lower error than the other bases when low-order approximation is used. In contrast, all spectral bases analyzed here, which are constructed using orthogonal polynomials (Lobatto, Legendre, and Chebychev), can converge to the reference solution as the polynomial order is increased.

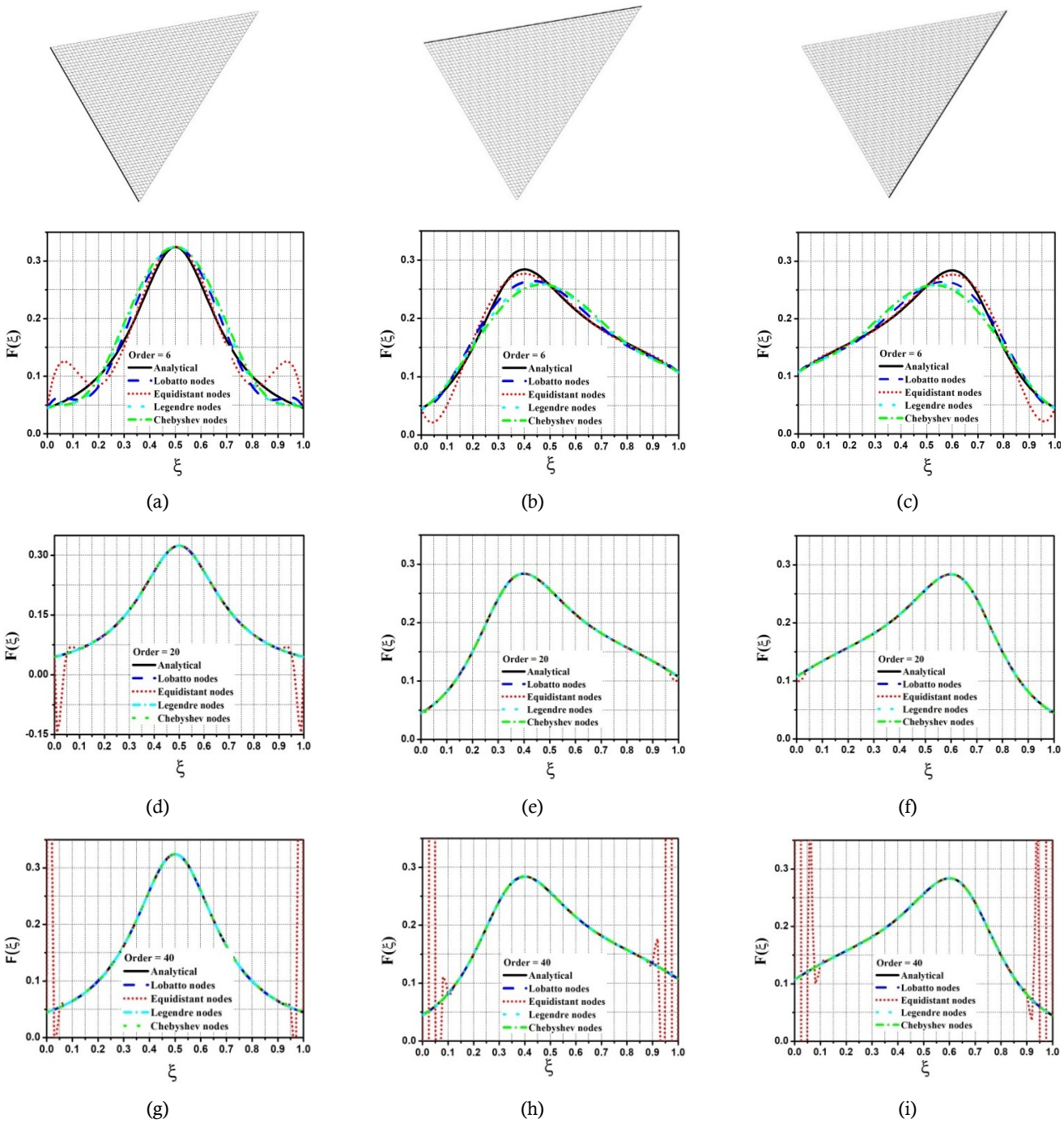

Fig. 5. Comparison between the nodal bases and the analytical function for each edge of the standard triangle.

Table 1. Lebesgue constant for random degrees of interpolation.

Order	Equidistant nodes	Lobatto nodes	Legendre nodes	Chebyshev nodes
2	1.2499	1.2499	1.2499	1.2499
3	1.6311	1.5140	2.0234	3.0550
4	2.2078	1.6358	2.1426	3.2370
5	3.1062	1.7785	2.4289	3.8284
6	4.5487	1.8737	2.5324	4.0137
7	6.9294	1.9723	2.6952	4.3333
8	10.938	2.0453	2.7753	4.4796
10	29.890	2.1804	2.9522	4.8153
20	109730	2.6064	3.4651	5.7840

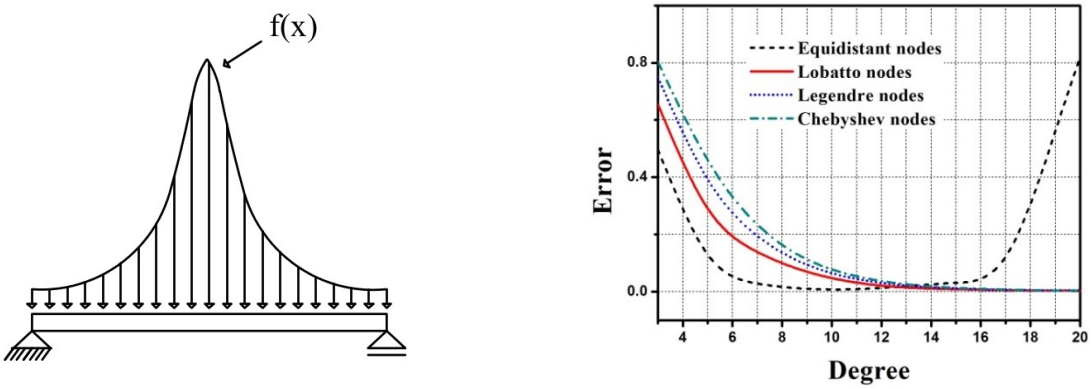

(a) (b)

Fig. 6. Simply supported beam subjected to loads with rapidly increasing behavior (a) and comparison between the nodal bases with respect to the error in the maximum displacement of the simply supported beam (b).

In Fig. 7a, a comparative study between the orthogonal bases (with degree equal 21) and equidistant base with degree equal 2 (Standard FEM), both with the same mesh (1 element), are analyzed. The results demonstrated the high accuracy of the orthogonal bases in recovering the analytical displacement field. The equidistant base with the degree of 2 (Standard FEM) however, differ significantly in relation to the analytical solution. Additionally, the equidistant base with a high order (m = 21), proved to be unstable when compared to orthogonal bases. Fig. 7b compares the computational cost for the nodal bases presented in this paper against the polynomial degree. While an increase in the polynomial degree necessitates more gauss points in the numerical integration, this has a negligible impact on computational cost across all nodal bases. The error in the stress field is shown in Fig. 8. Again, the orthogonal bases were able to stabilize at a high polynomial degree, while the equidistant base proved unstable in the analysis performed here.

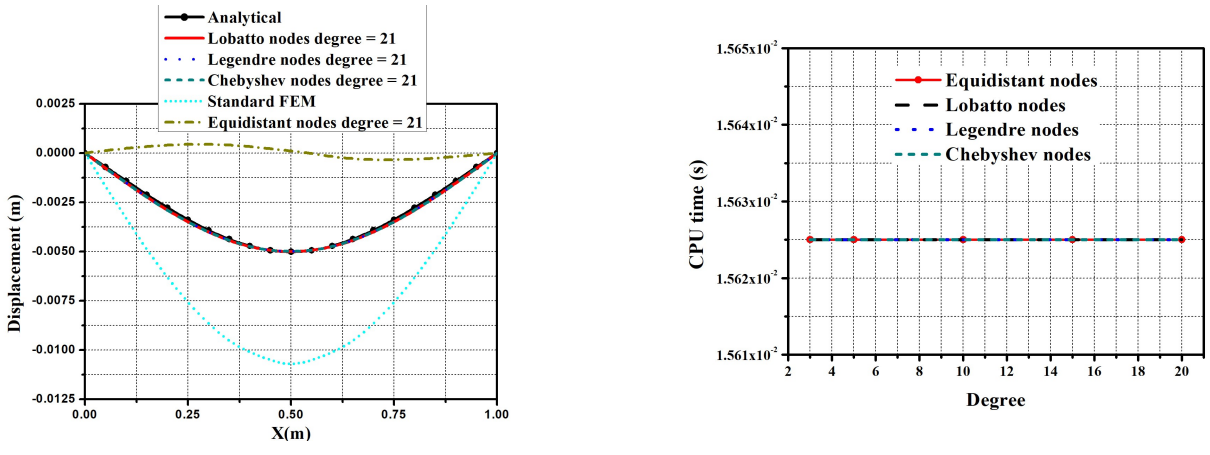

(a) (b)

Fig. 7. Comparison between the bases with respect to displacement field of the simply supported beam (a) and comparison between the nodal bases with respect to Computational efficiency (b).

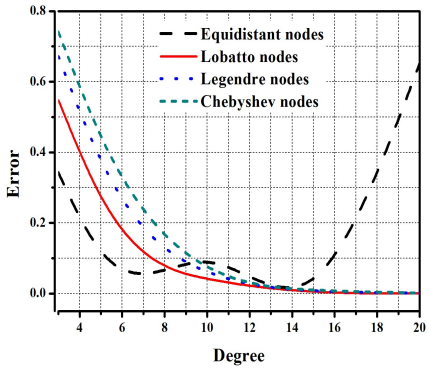

Fig. 8. Maximum error in stress field of the beam as the degree of approximation is increased.

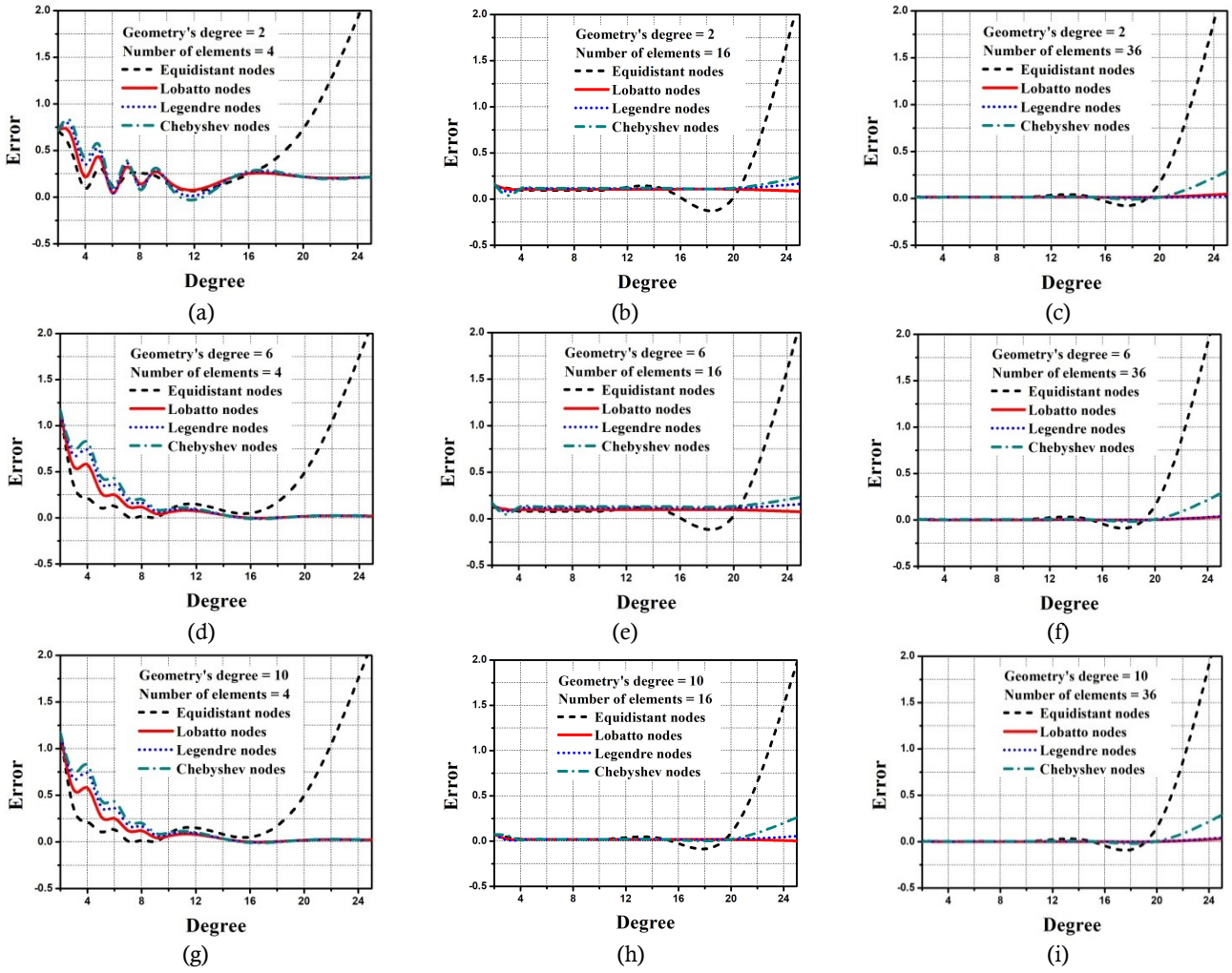

Fig. 9. Maximum displacement error as the number of elements and degree of approximation of both geometry and the load are varied.

6.3.2. Discretization of the simply supported beam: a 2D approach

The same structure and loading as those shown in Fig. 6 are analyzed using a 2D approach. In this paper, the influence in the displacement field is analyzed when the mesh, for both the structure and for the loading, is varied. During the analysis, the following information is used: modulus of elasticity, $E = 210GPa$, Poisson ratio, $\nu = 0.3$, beam length $L = 10m$, beam height $h = 1m$, and thickness $t = 1m$.

In this study, the variation in the maximum displacement error (ordinate axis) is analyzed as the following parameters are varied: degree of approximation of the load (abscissa axis), degree of approximation, and number of triangular elements in the discretization of the problem domain. Fig. 9 shows that the change in the degree of approximation of the structure, here called geometry's degree, does not interfere in the displacement error analysis. However, the displacement results are sensitive to the variation in the number of elements. Another evaluation from Fig. 9 is that for a

lesser number of mesh elements, the displacement field errors are insignificant when a high-order spectral base is used, but not when the equally spaced high-order base is applied. However, as the number of elements in the mesh is increased and the degree of loading approximation is varied, one can observe that the equally spaced base continues to provide inconsistent results in addition to the fact that the Chebychev base provides small errors when the order of approximation is above 20, which is not the case for Legendre and Lobatto bases.

A comparative analysis between the orthogonal bases (with the geometry's degree of 10 and the loading approximation of 20) and the equidistant base with degree equal 2 for geometry and loading approximation (Standard FEM) is carried out. In Fig.10a, the stability of the orthogonal basis in recovering the solution, even with a poor mesh, is shown. The equidistant base with degree equal 20 observes higher error when the mesh is lower. In addition, the equidistant base provided inconsistent results even when the mesh was increased. This poor performance can be attributed to Runge phenomenon. As we increase the number of elements, the standard FEM converges to reference solution with a minimum of 35 elements. In Fig. 10b, while the computational cost for standard FEM remained unchanged as the number of elements increases, the orthogonal bases observed a significant increase in CPU time. In Fig. 11, the characteristics of all nodal bases in recovering the stress field with both mesh and geometry's degree fixed (4 and 10 respectively) is presented. As can be seen, the orthogonal bases succeeded in stabilizing when the degree was above 10, while the equidistant base observed significant error.

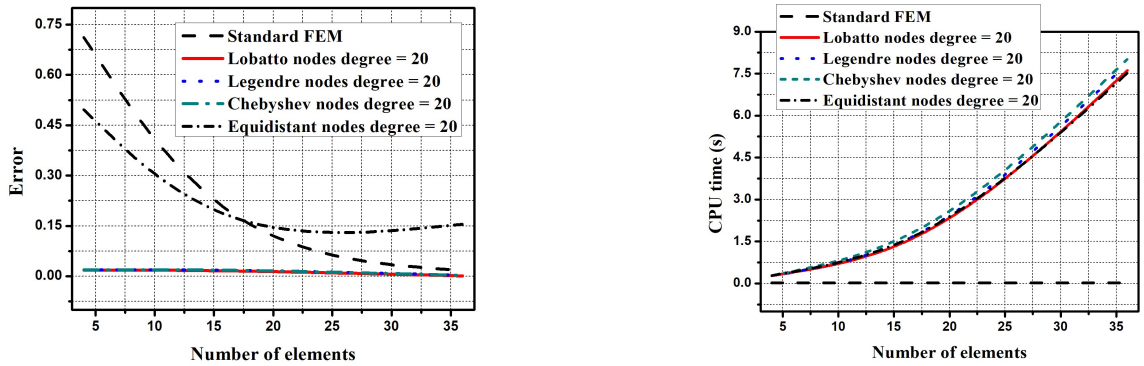

(a) (b)

Fig. 10. Comparative study in maximum displacement error between the orthogonal bases and the standard FEM as the number of elements increases (a) Computational cost as the number of elements enhance for all the orthogonal bases and the standard FEM (b).

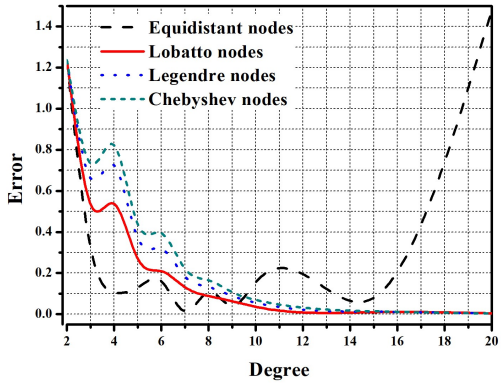

Fig. 11. Maximum **e**rror in the stress field for all the nodal bases when the degree increases.

6.3.3. Elastostatic analysis of a gear: a 2D approach

The geometrical design of a mechanical gear, and in detail, the representative element of the tooth, as well as the imposition of the loading described by Eq. (30), is shown in Fig. 12.

In this example, the geometry of the gear includes an internal diameter of 32 mm and an external diameter of 34 mm. The loading, represented by Eq. (30) is applied perpendicular to the region marked in red in Fig. 12. Both horizontal and vertical displacement are restricted at point A and B (see Fig. 12). For numerical analysis, the reference solution consists of 22,000 triangular elements with a degree of approximation equal to 2 for the domain mesh and 112 1D elements for discretizing the load are constructed using the Abaqus software. In the analysis of the efficiency of the spectral bases compared to the equally spaced base, a mesh formed by two triangular elements is used to describe the gear's geometry and a 1D single element is used to describe the loading.

For the present example, which has complexity in both the geometric and load representations, it can be seen (Fig. 13) that only the spectral base of Lobatto, from a degree of approximation of 9, presents excellent stability in convergence for the reference solution. The other bases differ significantly in relation to the reference solution even when a high degree of approximation is used. In addition, the standard FEM (equidistant nodes with degree equal 2) observed a significantly higher error when compared to Lobatto base with degree equal 20. For this analysis, the degrees of approximation for both geometry and loading are varied equally.

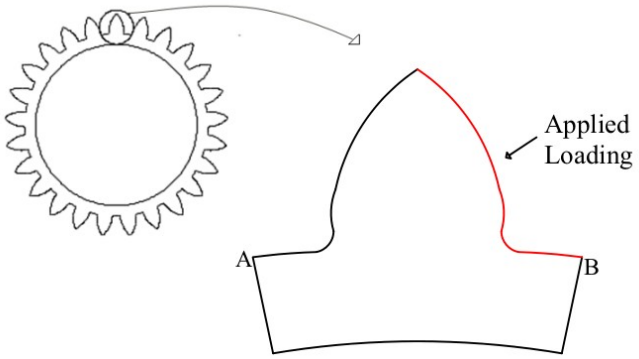

Fig. 12. Geometric representation of the gear

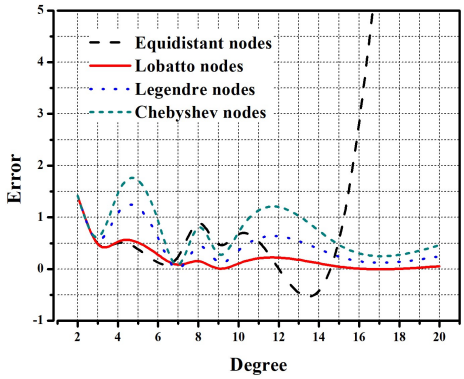

Fig. 13. Maximum displacement error for the gear subjected to a load with gradient of intensity

In Fig. 14a, the error in the stress field is shown. It can be observed that the orthogonal bases obtained a good performance when the order was increased higher than 10, and excellent stability in recovering the reference solution when both geometry's and loading degree was high. On the contrary, the equidistant base proved unstable in capturing the stress field. In Fig. 14b, the relationship between computational cost of all nodal bases to the degree of approximation is shown. As can be observed, none of the nodal bases observed significant computational cost when the degree was less than 8. When the order was further increased however, a considerable increase in computational cost can be observed for all the bases, with the rate of increase approximately the same for each.

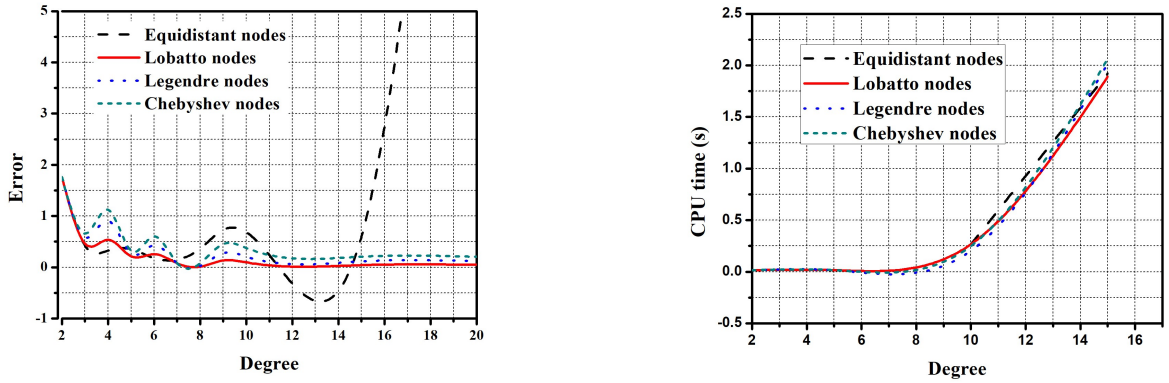

Fig. 14. Maximum error in the stress field for the gear subjected to a load with gradient of intensity (a) and the CPU time for all the nodal bases as the degree increases.

7. Conclusion

The analysis of the spectral interpolation applied to FEM is presented for 1D and 2D elastostatic problems. The spectral interpolation is constructed from the nodal bases formed by zeros of the orthogonal polynomials. In this paper, a comparative study was carried out between the bases generated by Legendre, Lobatto, and Chebychev polynomials and a base constructed with equally spaced nodes, the latter being commonly used. In both the 1D and 2D approaches, the shape functions used in the FEM were constructed using the generalized Vandermonde matrix. In addition, 2D interpolation was performed using Proriol's function imposed on the positions of the nodal bases (Legendre, Lobatto, Chebychev, and equally

spaced), and for the 1D approach, a complete Lagrange-type polynomial was used.
Considering the nodal bases, it is observed that the error in the interpolation process is directly related to the position of the interpolating nodes, which can be represented by the following parameters: the Lesbegue constant and the condition number of the generalized Vandermonde matrix (Fig. 4).
In the present paper, a comparative study between the low- and high-order nodal bases is performed using the Lebesgue constant, condition number, and relative error. In this study, structures with complex geometries (gear) and loaded with rapid increases are analyzed. The results indicate that the high-order spectral base, especially that of Lobatto, is significantly efficient compared to the equally spaced base, when 1D or 2D elastostatic problems with complex geometries and subjected to loads with gradient of intensity are analyzed. It is observed that the Lobatto base provides a lower Lebesgue constant and condition number when compared to all other bases presented in this study. Fig. 13 shows the efficiency of Lobatto approximation with fewer elements (with two triangular elements for the structure mesh and a single 1D element for loading) as the order of approximation is high, which is not the case for other bases.
In all examples presented in this paper, a comparative study between the high-order bases and the standard FEM with the same mesh is performed. The standard FEM proved to be less successful in the recovery of solutions with a less refined mesh, while the orthogonal bases showed improved efficiency with a significantly lower requirement in mesh discretization. In terms of computational time, the orthogonal bases presented higher computational cost when the geometry's degree (Fig. 14b) and the mesh discretization (Fig. 10b) was increased, while the standard FEM observed a low computational cost regardless. In the 1-D case (Fig. 7b), the spectral bases matched the computational cost of the standard FEM even when the degree was increased. The increase in CPU time when the nodal bases with higher degree was used is due to the necessity for more gauss points, however this is only observed in the 2-D approach.
In view of the presented results, we can observe that the spectral base of Lobatto, together with FEM, is significantly efficient and cost- effective for both 1D and 2D problem analysis, especially in the 1-D analysis, and it is desired to use fewer elements and a high order in the degree of approximation.

Acknowledgments

The authors would like to acknowledge Coordenação de Aperfeiçoamento de Pessoal de Nível Superior – Brasil (CAPES) – Finance code 001 for the financial support.

Conflict of Interest

The authors declared no potential conflicts of interest with respect to the research, authorship and publication of this article.

Funding

The authors received no financial support for the research, authorship and publication of this article.

References

[1] Babuska, I., Szabo, B.A., Katz, I.N., The p-version of the finite element method. *SIAM Journal on Numerical Analysis*, 18(3), 1981, 515-545.
[2] Rocha, F.C., Kzam, A.K.L., Análise das aproximações de alta ordem por meio da interpolação espectral aplicadas ao MEC potencial. In *proceeding XXXIV Iberian Latin-American Congress in Computational Methods in Engineering*, 2013.
[3] Zak, A., Krawczuk, M., Certain numerical issues of wave propagation modelling in rods by the Spectral Finite Element Method. *Finite Elements in Analysis and Design*, 47, 2011, 1036-1046.
[4] Kudela, P., et al. Wave propagation modelling in 1D structures using spectral finite elements. *Journal of Sound and Vibration*, 300(1-2), 2007, 88-100.
[5] Karniadaki, G. E., Sherwin, S. J., Spectral/Hp Element Methods for CFD. Oxford: Oxford University Press, 1999.
[6] Nogueira, A.C. Jr., Bittencourt, M.L., Spectral/HP finite elements applied to linear and non-linear structural elastic problems. *Latin American Journal of Solids and Structures*, 4, 2007, 61-85.
[7] Willberg, C., Duczek, S., Vivar Perez, J.M., Schmicker, D., Gabbert, U., Comparison of different higher order finite element schemes for the simulation of lamb waves. *Computer Methods in Applied Mechanics and Engineering*, 241, 2012, 246-261.
[8] Fornberg, B., and Julia, Z., The Runge phenomenon and spatially variable shape parameters in RBF interpolation. *Computers & Mathematics with Applications*, 54(3), 2007, 379-398.
[9] Brutman, L., Lebesgue functions for polynomial interpolation, a survey. *Annals of Numerical Mathematics*, 4, 1997, 111-127.
[10] Vos, P.E.J., Sherwin, S.J., Kirby, R.M., From h to p efficiently: implementing finite and spectral/hp element methods to achieve optimal performance for low- and high-order discretisations. *Journal of Computational Physics*, 229(13), 2010, 5161-5181.
[11] Sherwin, S.J., Karniadakis, G.E., A triangular element method; applications to the imcompressible Navier-Stokes equations. *Computer Methods in Applied Mechanics and Engineering*, 123(1–4), 1995, 189-229.

[12] Sherwin, S.J., Karniadakis, G.E., Tetrahedral hp finite elements: algorithms and flow simulations. *Journal of Computational Physics*, 124, 1996, 14-45.
[13] Tai, C.-Y., & Chan, Y. J. A hierarchic high-order Timoshenko beam finite element. *Computers & Structures*, 165, 2016, 48-58.
[14] W. Dauksher, A.F. Emery, The solution of elastostatic and elastodynamic problems with Chebyshev spectral finite elements, *Computer Methods in Applied Mechanics and Engineering*, 188, 2000, 217-33.
[15] Khaji, N., & Zakian, P. Uncertainty analysis of elastostatic problems incorporating a new hybrid stochastic-spectral finite element method. *Mechanics of Advanced Materials and Structures*, 24(12), 2016, 1030-1042.
[16] Man, H., Song, C., Xiang, T., Gao, W., & Tin-Loi, F. High-order plate bending analysis based on the scaled boundary finite element method. *International Journal for Numerical Methods in Engineering*, 95(4), 2013, 331-360.
[17] Man, H., Song, C., Gao, W., & Tin-Loi, F. Semi-analytical analysis for piezoelectric plate using the scaled boundary finite-element method. *Computers & Structures*, 137, 2014, 47-62.
[18] Lin, G., Zhang, P., Liu, J., & Li, J. Analysis of laminated composite and sandwich plates based on the scaled boundary finite element method. *Composite Structures*, 187, 2018, 579-592.
[19] Zak, A., & Krawczuk, M. Static and dynamic analysis of isotropic shell structures by the spectral finite element method. *Journal of Physics: Conference Series*, 382, 2012, 012054.
[20] Wang, Q., Sprague, M.A., Legendre spectral finite element implementation of geometrically exact beam theory, in: *Proceedings of the 54th AIAA/ASME/ASCE/AHS/ASC Structures, Structural Dynamics, and Materials Conference*, National Harbor, USA, 2013.
[21] Proriol, J., Sur une famille de polynomes à deux variables orthogonaux dans um triangle. *Comptes Rendus Mathematique Academie des Sciences*, 245(26), 1957, 2459-2461.
[22] Fejer, L. Lagrangesche interpolation und die zugehorigen konjugierten punkte. *Mathematische Annalen*, 106, 1932, 1-55.
[23] Blyth, M. G., & Pozrikidis, C. A Lobatto interpolation grid over the triangle. *IMA Journal of Applied Mathematics*, 71(1), 2016, 153-169.
[24] Pozrikidis, C., *Introduction to Finite and Spectral Element Methods Using Matlab*. Chapman & Hall/CRC, 2005.
[25] Franco, N. B., *Cálculo numérico*, São Paulo: Pearson Prentice Hall, 2007.
[26] Oñate, E., *Structural Analysis with the Finite Element Method. Linear Statics*. 1st ed. Barcelona: Springer, 2013.
[27] Ostachowicz, W., Kudela, P., Krawczuk, M., Zak, A., *Guided Waves in Structures for SHM: The Time-domain Spectral Element Method*. John Wiley & Sons Ltd: Chichester, UK, 2011.
[28] Blyth, M.G., Pozrikidis, C. A., Lobatto interpolation grid over the triangle. *IMA Journal of Applied Mathematics*, 71, 2006, 153-169.
[29] Pozrikidis, C.A., Spectral-element method for particulate Stokes flow. *Journal of Computational Physics*, 156, 1999, 360-381.
[30] Rivlin, T.J., *An introduction to the approximation of functions*. Dover Publications; Revised edition, 1969.
[31] Reddy, J.N., On locking-free shear deformable beam finite elements. *Computer Methods in Applied Mechanics and Engineering*, 149(1-4), 1997, 113-132.
[32] Brebbia, C. A., *The Boundary element Method for Engineers*. London: Pentech Press, 1978.
[33] Hughes, T. J. R., *The Finite Element Analysis*. Prentice-Hall. New Jersey, 1987.
[34] Szabi, B., Babuska, I. *Finite element analysis*. Wiley. New York, 1991.
[35] Zienkiewicz, O. C., Taylor, R. L., *The Finite Element Method*. Fourth Ed. McGraw-Hill. New York, 1989.

© 2020 by the authors. Licensee SCU, Ahvaz, Iran. This article is an open access article distributed under the terms and conditions of the Creative Commons Attribution-NonCommercial 4.0 International (CC BY-NC 4.0 license) (http://creativecommons.org/licenses/by-nc/4.0/).